Electronic Supplementary Material (ESI) for Journal of Materials Chemistry B.

Supporting Information

Mace-like Heterostructural Enriched Injectable Hydrogel Composite for On-demand Promotion of Diabetic Wound Healing

Li Wang,[1,2] Zahid Hussain,[1,2] Penghui Zheng,[2] Yajie Zhang,[2] Yi Cao,[2] Tong Gao,[2] Zhuangzhuang Zhang,[1,2] Yuehu Zhang, [2] Renjun Pei[1,2]*

[1]School of Nano-Tech and Nano-Bionics, University of Science and Technology of China, Hefei, 230026, China.

[2]CAS Key Laboratory for Nano-Bio Interface, Suzhou Institute of Nano-Tech and Nano-Bionics, Chinese Academy of Sciences, Suzhou, 215123, China

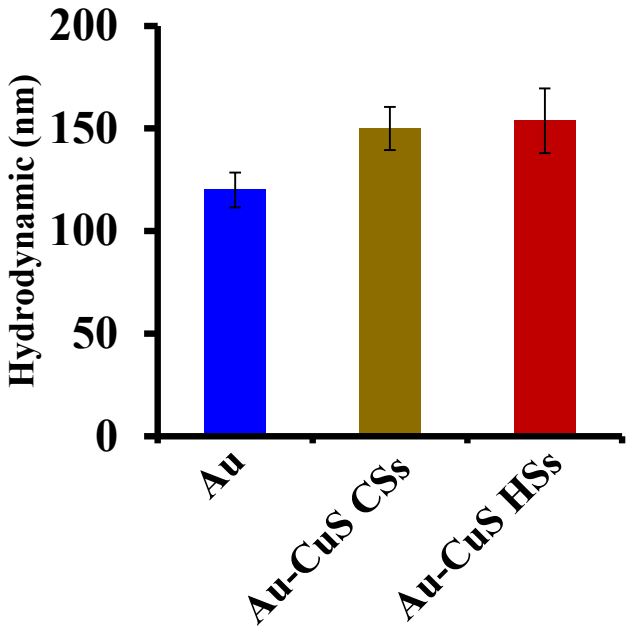

Figure S1. The hydrodynamic sizes of Au, Au-CuS CSs, and Au-CuS HSs in water.

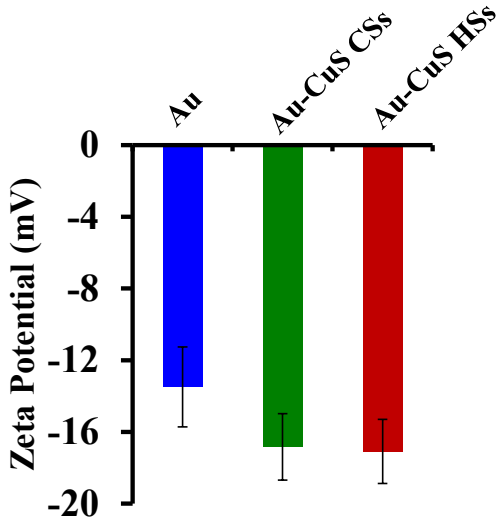

Figure S2. The Zeta potentials of Au, Au-CuS CSs, and Au-CuS HSs in water.

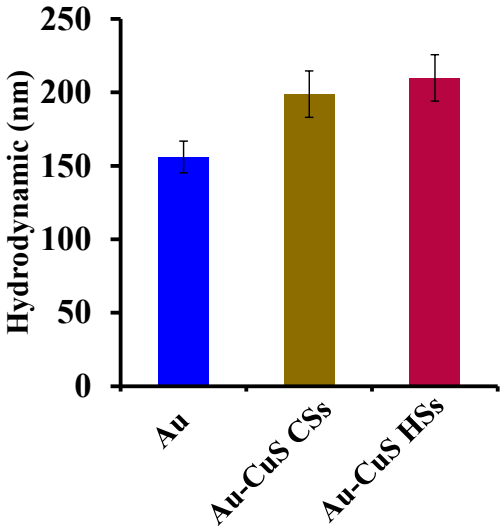

Figure S3. The hydrodynamic sizes of the different facets Au, Au-CuS CSs, and Au-CuS HSs in DMEM culture medium containing 10% FBS.

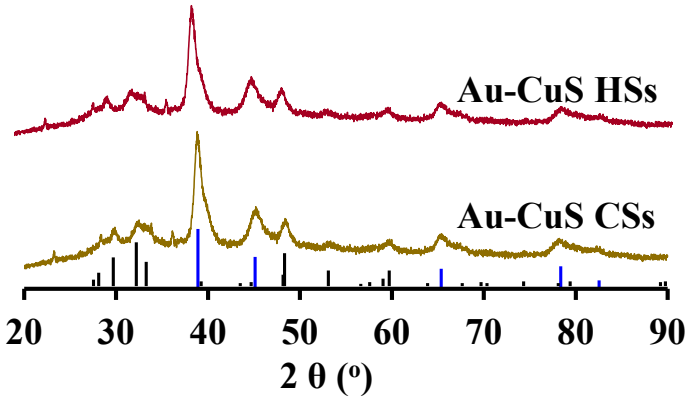

Figure S4. XRD pattern of Au-CuS CSs and Au-CuS HSs**.** The blue line represents the standard cubic phase of Au (JCPDS No. 04-0784) and the black line is for the standard covellite phase of CuS (JCPDS No. 06-0464).

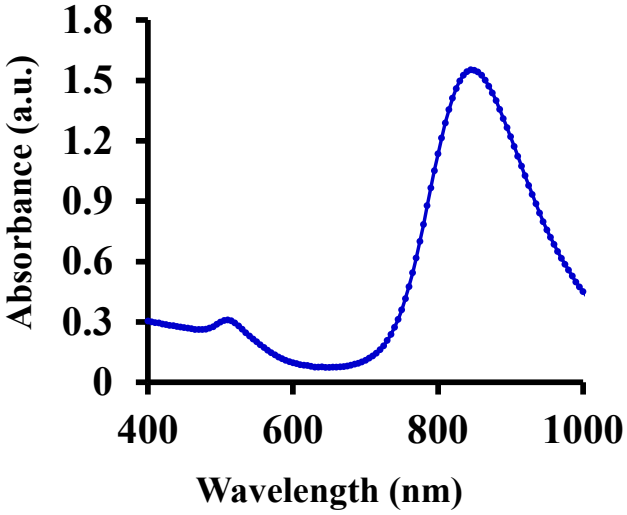

Figure S5. UV-Vis-NIR absorption spectra of Au NRs.

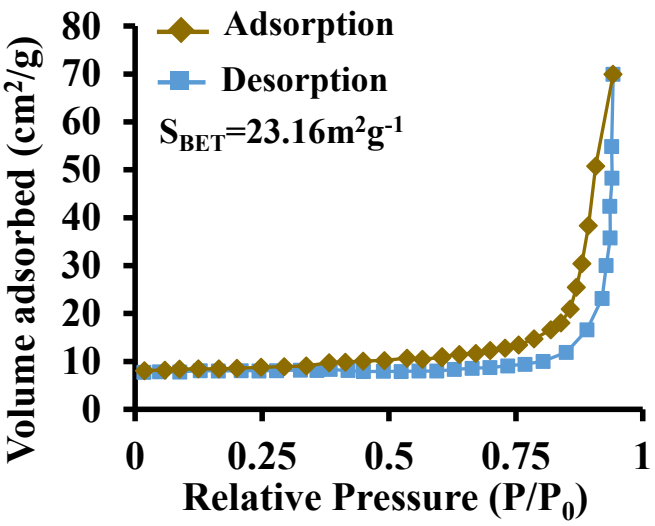

Figure S6. Determination of the specific surface area of Au-CuS CSs.

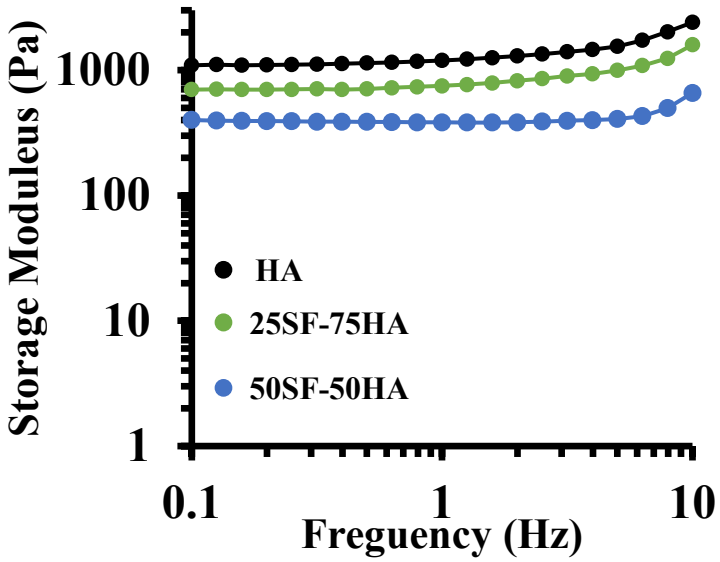

Figure S7. Storage modulus-strain response patterns of HA，25SF-75HA and 50SF-50HA hydrogels.

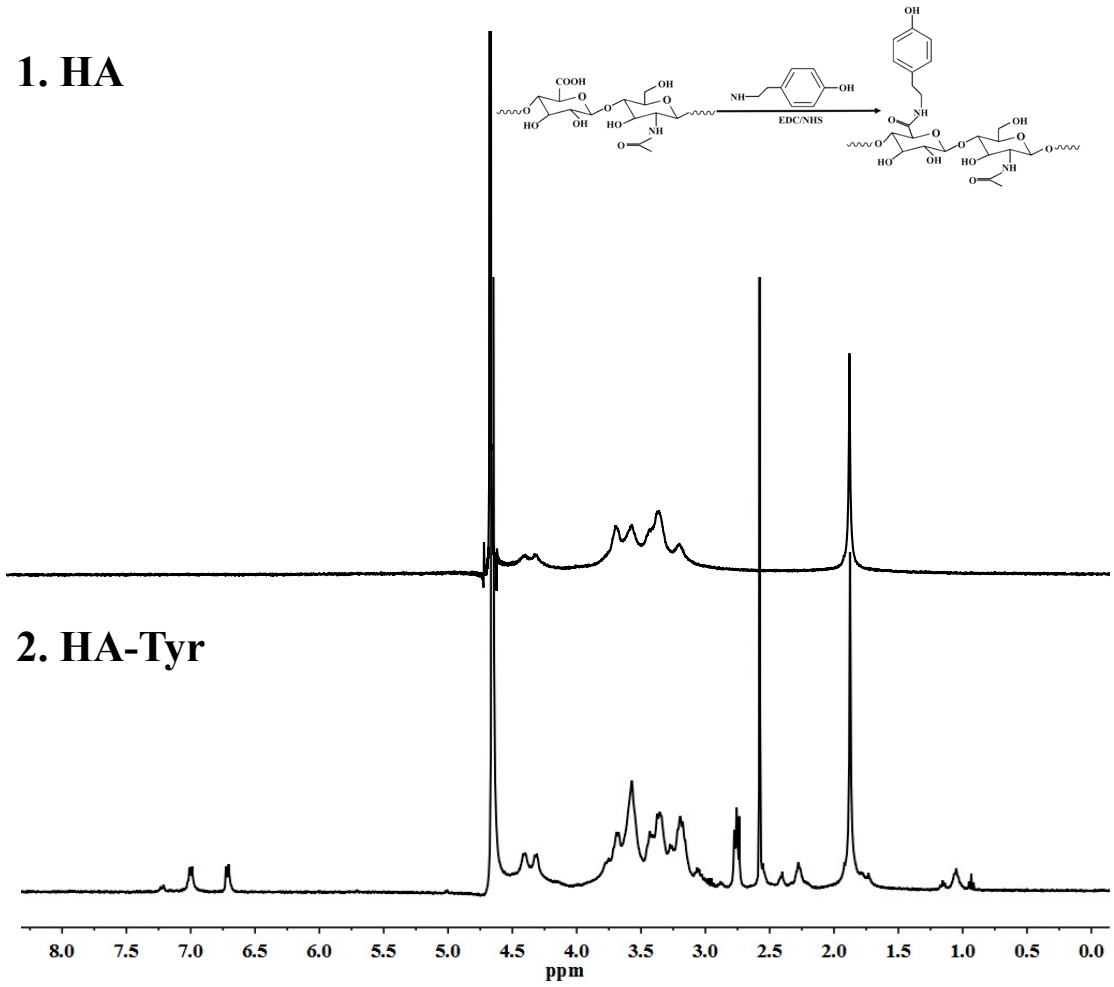

Figure S8. ^{1}H NMR of HA and HA-Tyr.

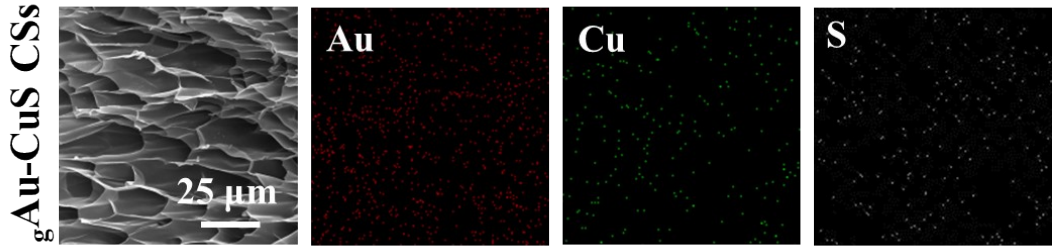

Figure S9. Representative SEM image and corresponding EDX elemental mappings of gAu-CuS CSs hydrogel

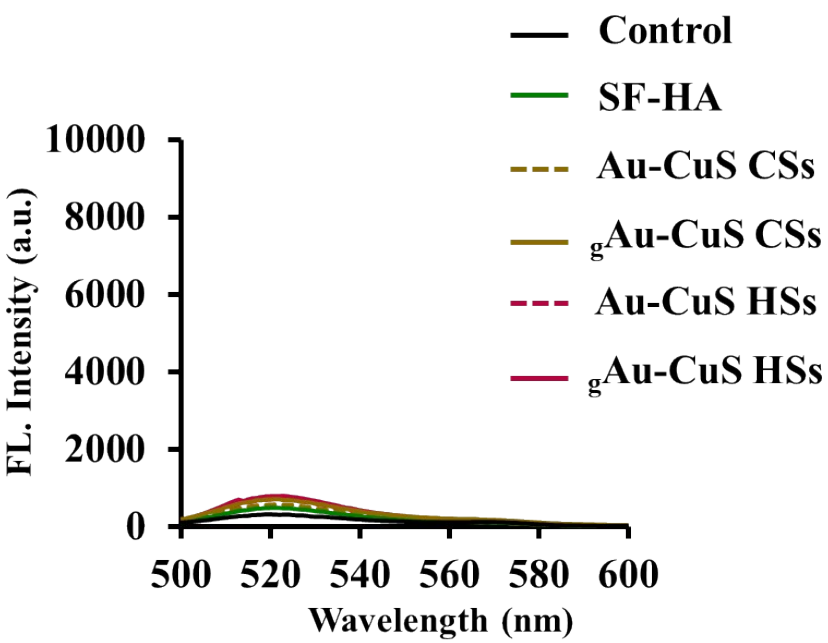

Figure S10. Emission spectra of DCF in PBS solution after 12 h of incubation with 100 μg mL^{-1} gAu-CuS CSs hydrogel and gAu-CuS HSs hydrogel (equivalent to Au-CuS) without NIR laser irradiation. Excitation wavelength-455 nm.

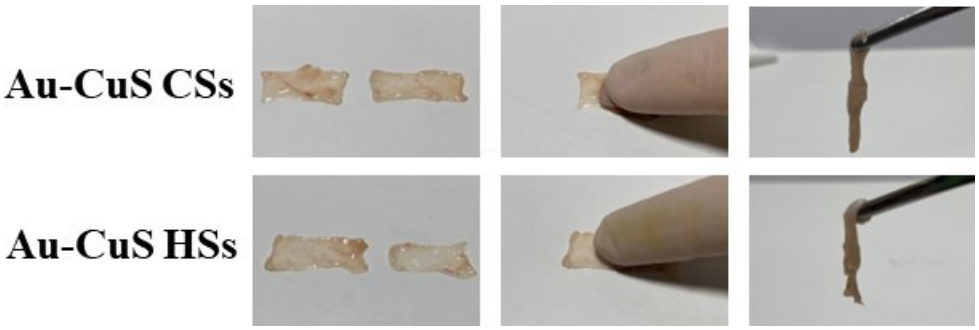

Figure S11. Adhesion properties of Au-CuS CSs and Au-CuS HSs on two pieces of the mouse skin.

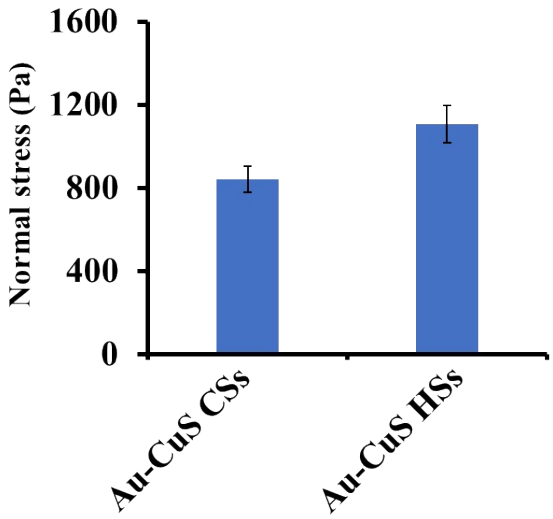

Figure S12. The adhesive strength of Au-CuS CSs and Au-CuS HSs toward skin tissue was evaluated via a lap-shear test.

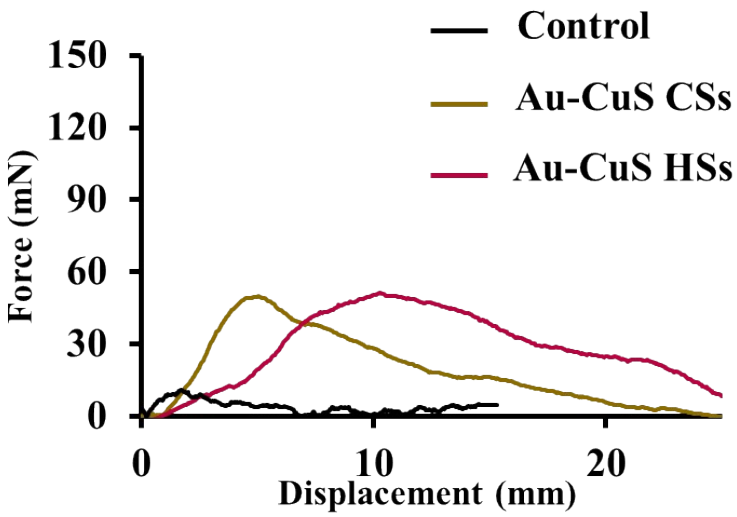

Figure S13. Force–displacement curves for lap joints of two mouse skins glued by Au-CuS CSs and Au-CuS HSs.

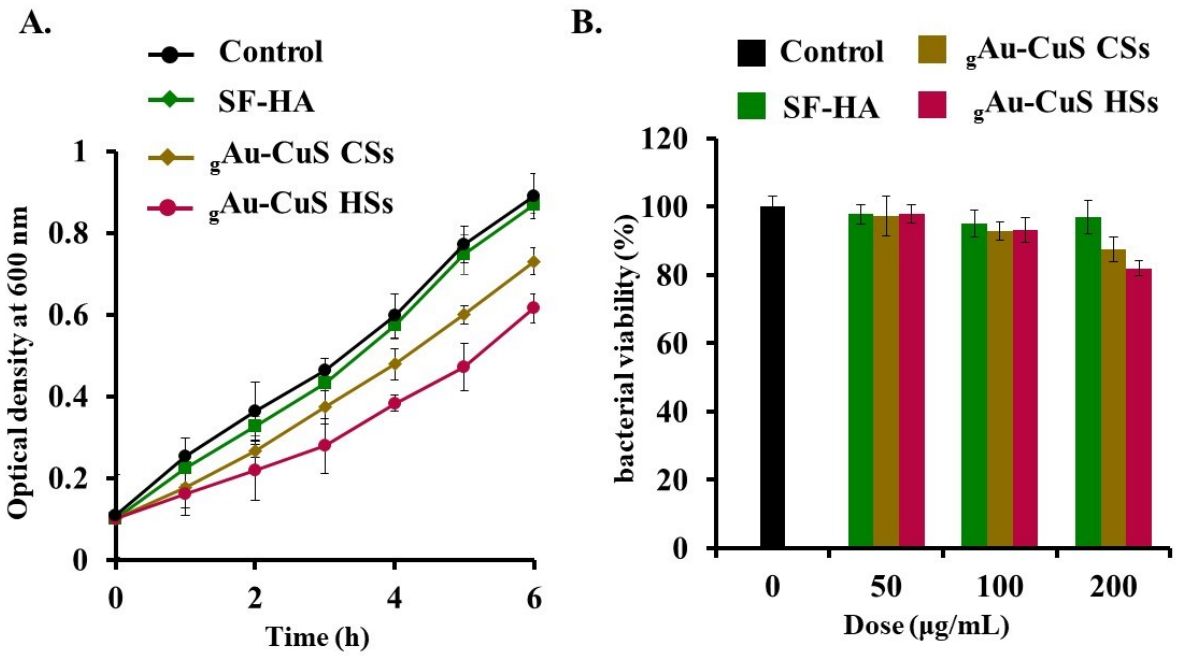

Figure S14. Bacterial growth curves (A) and viability (B) of *E. coli* treated with 50 μg mL^{-1} gAu-CuS CSs hydrogel and gAu-CuS HSs hydrogel (equivalent to Au-CuS) without NIR laser.

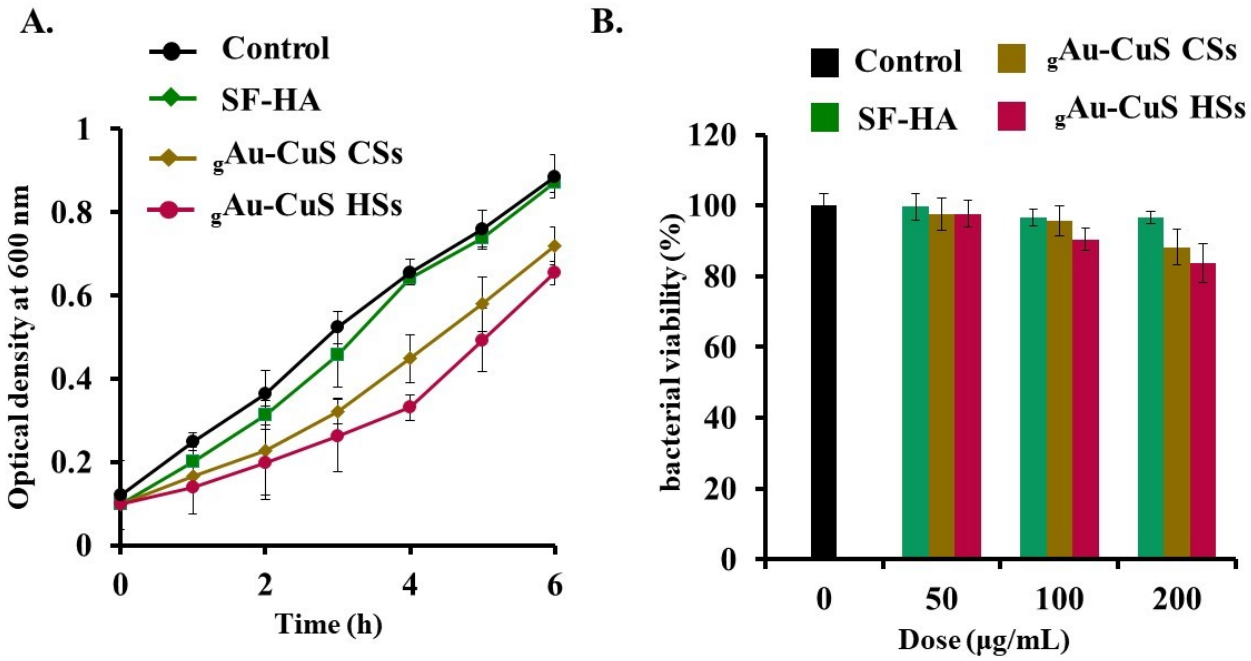

Figure S15. Absorbance at 600 nm of bacteria (A) and viability (B) of *S. aureus* treated with 50 μg mL^{-1} gAu-CuS CSs hydrogel and gAu-CuS HSs hydrogel (equivalent to Au-CuS) without NIR laser.

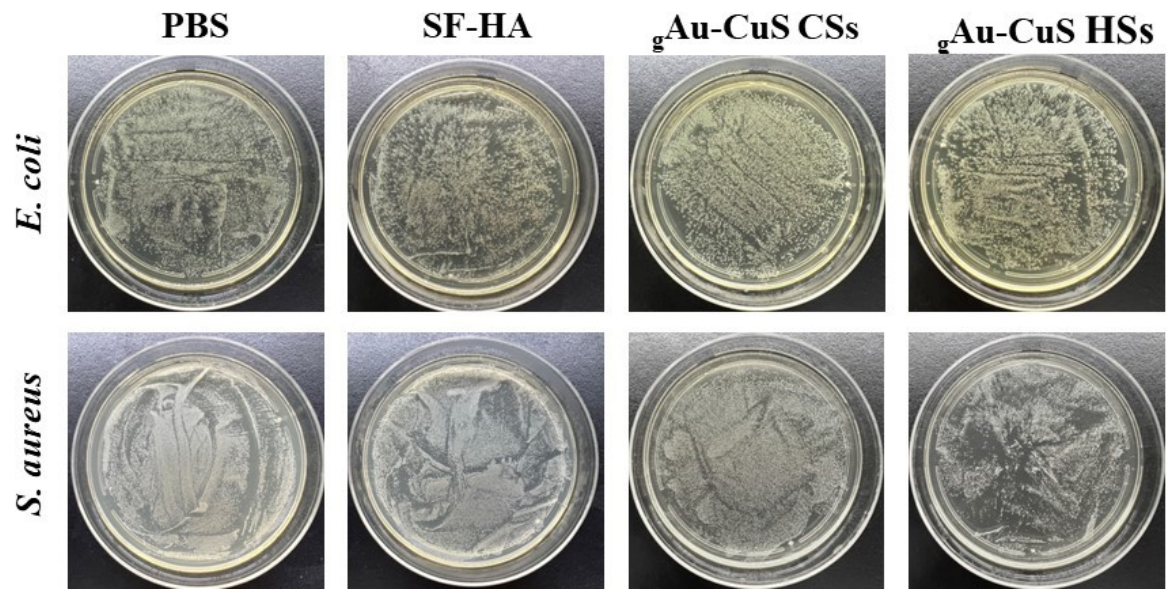

Figure S16. Petri dish photographs showed bacterial CFU of *E. coli* and *S. aureus* treated with 50 μg mL^{-1} gAu-CuS CSs hydrogel and gAu-CuS HSs hydrogel (equivalent to Au-CuS) without NIR laser.

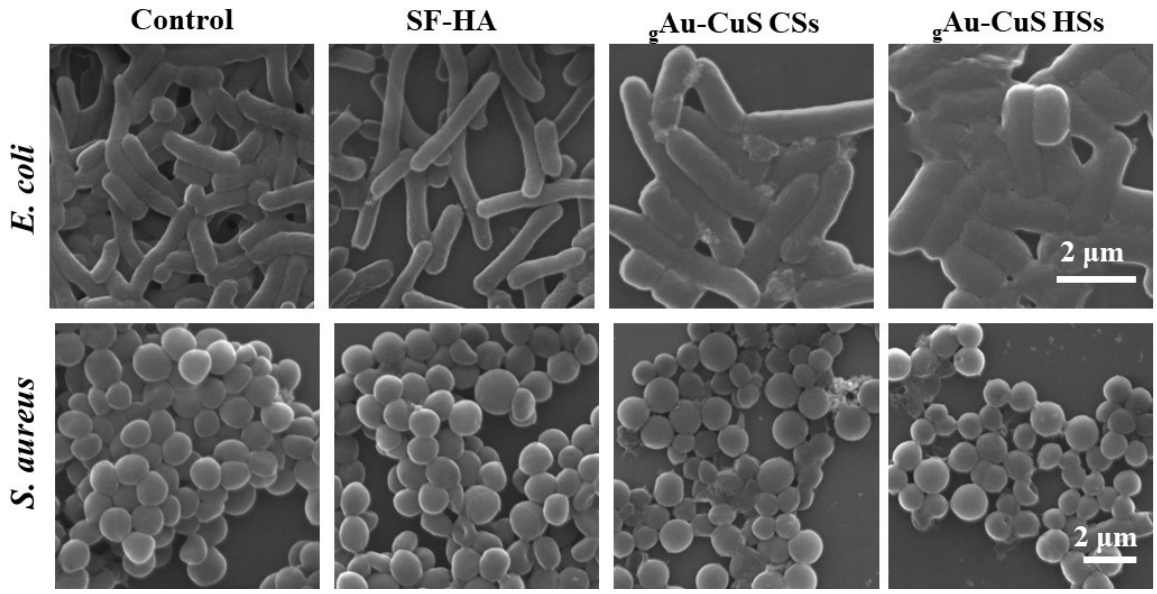

Figure S17. SEM images of *E. coli* and *S. aureus* were treated with 50 μg mL^{-1} gAu-CuS CSs hydrogel and gAu-CuS HSs hydrogel (equivalent to Au-CuS) without NIR laser.

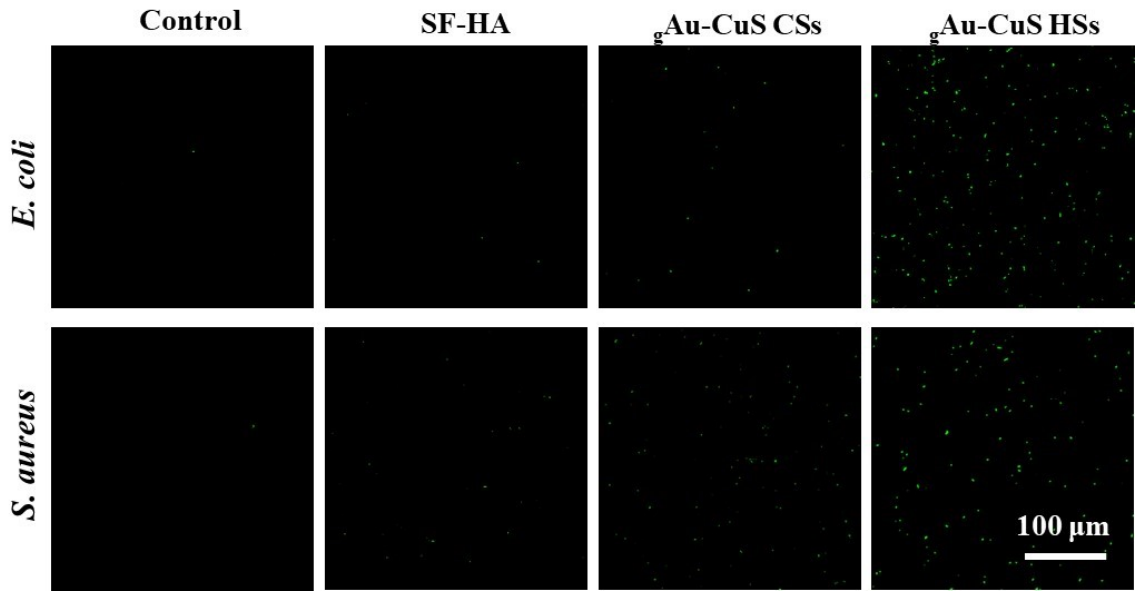

Figure S18. DCF fluorescence intensities of *E. coli* and *S. aureus* treated with 50 μg mL^{-1} gAu-CuS CSs hydrogel and gAu-CuS HSs hydrogel (equivalent to Au-CuS) without NIR laser irradiation.

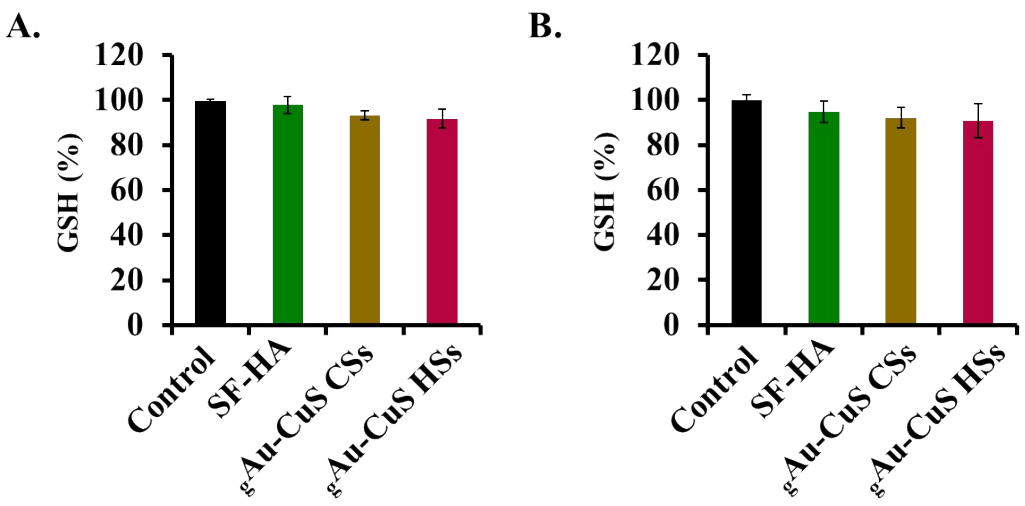

Figure S19. GSH levels of *E. coli* and *S. aureus* treated with 50 μg mL^{-1} gAu-CuS CSs hydrogel and gAu-CuS HSs hydrogel (equivalent to Au-CuS) without NIR laser irradiation.

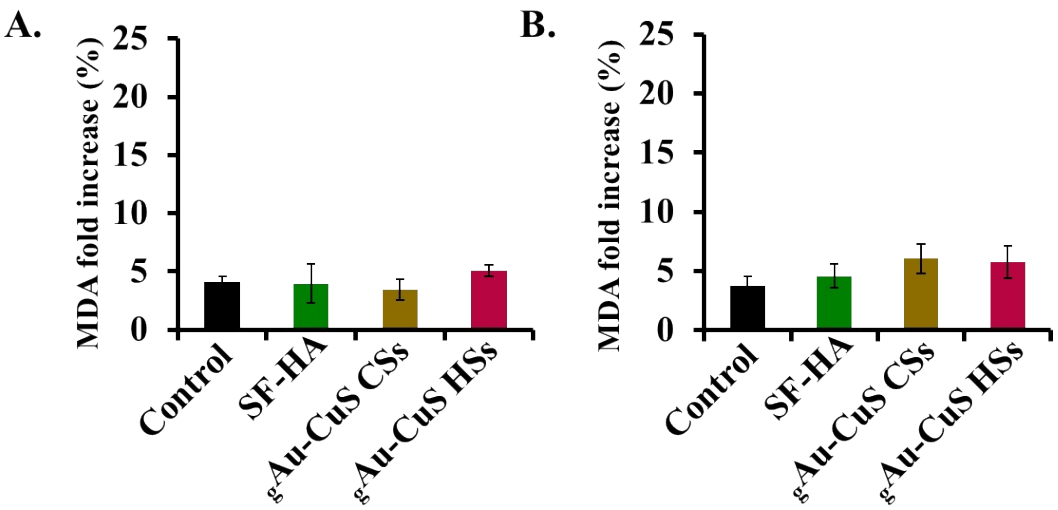

Figure S20. Lipid peroxidation levels of *E. coli* and *S. aureus* treated with 50 μg mL^{-1} gAu-CuS CSs hydrogel and gAu-CuS HSs hydrogel (equivalent to Au-CuS) without NIR laser irradiation.

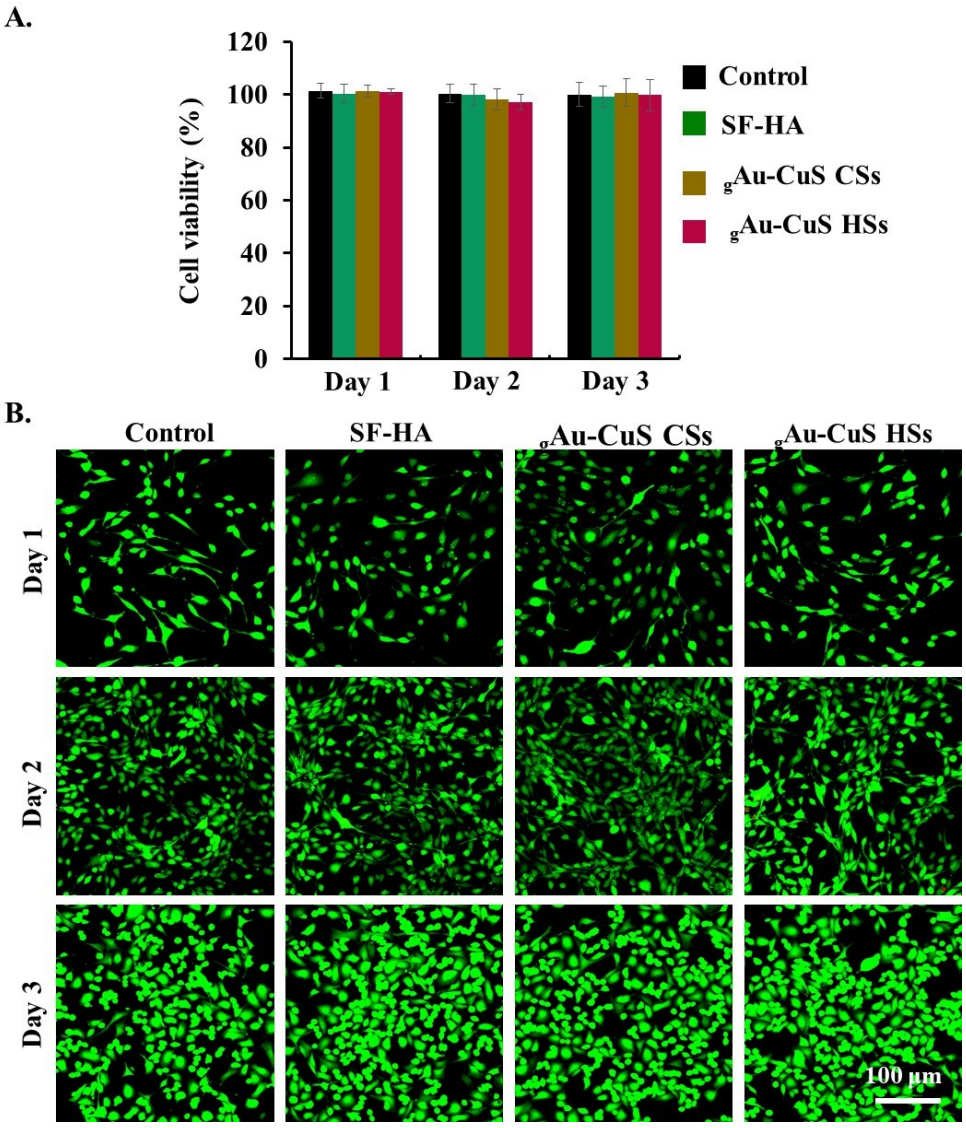

Figure S21. (A) Viability assessment of 3T3 cells treated with 100 μg mL^{-1} gAu-CuS CSs hydrogel and gAu-CuS HSs hydrogel (equivalent to Au-CuS) for 24 h, 48h or 72 h without NIR laser irradiation and assessed by MTT assay. (B) Live/dead cell staining of 3T3 cells treated with 100 μg mL^{-1} gAu-CuS CSs hydrogel and gAu-CuS HSs hydrogel (equivalent to Au-CuS) for 24 h, 48h or 72 h without NIR laser irradiation.

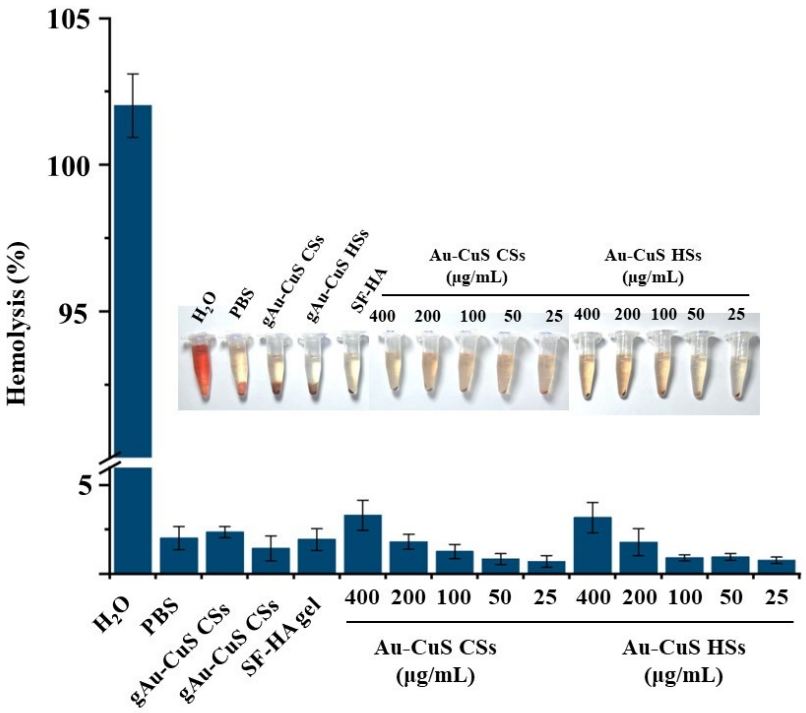

Figure S22. Hemolysis of gAu-CuS HSs hydrogel and different components. Hemolytic ratio of gAu-CuS CSs hydrogel, gAu-CuS HSs hydrogel, Au-CuS CSs and Au-CuS HSs (10, 20, 50, 100, 200, 400 μg mL^{-1}). Inset: digital photograph of hemolytic test, Error bar represent mean ± SD, n=3.

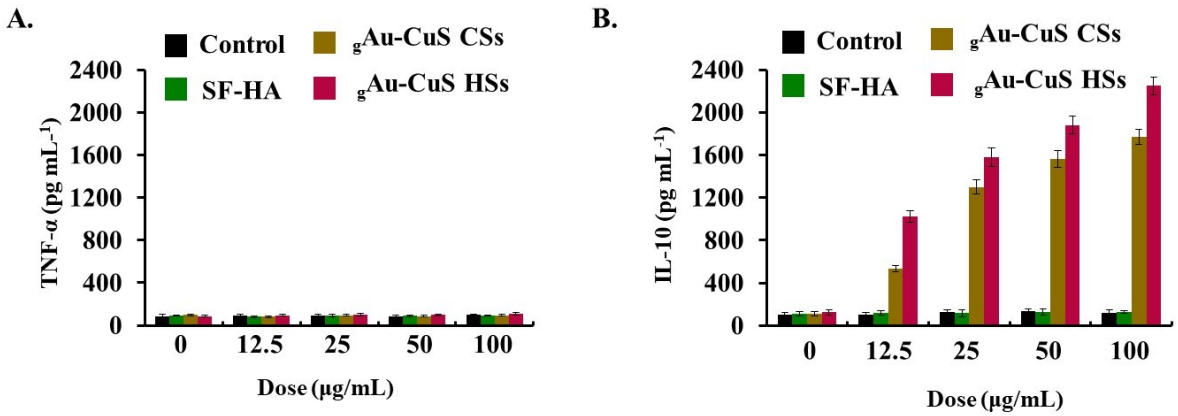

Figure S23. Levels of TNF-α A) and IL-10 factor (B) expression in cells after RAW 264.7 was treated with different concentration of gAu-CuS CSs hydrogel and gAu-CuS HSs hydrogel (equivalent to Au-CuS) without NIR laser irradiation.

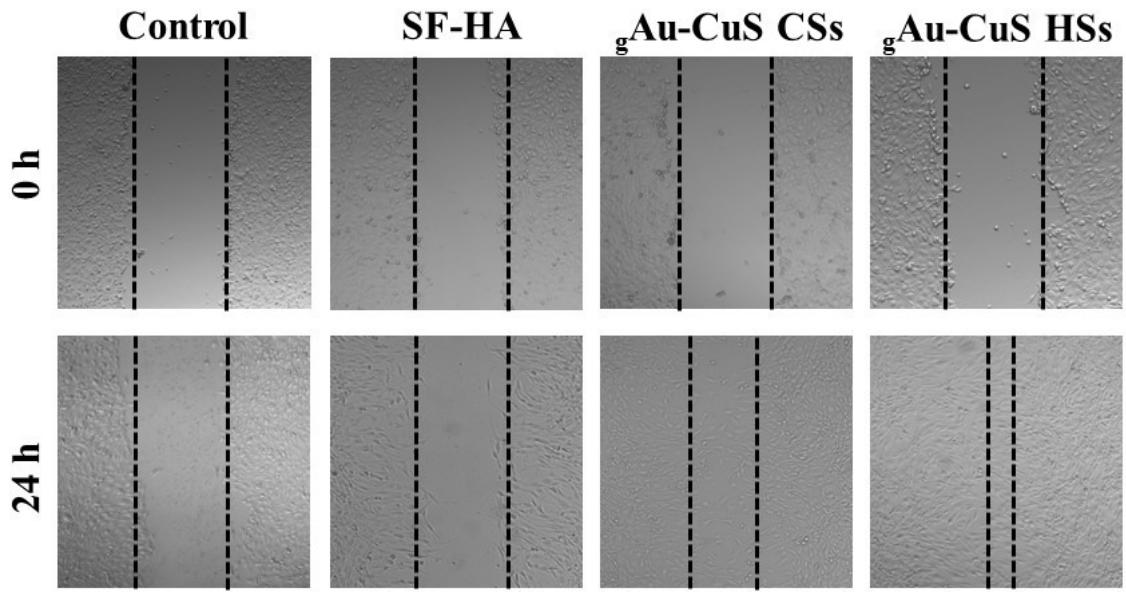

Figure S24. Level of cell migration after treatment with 100 μg mL^{-1} gAu-CuS CSs hydrogel and gAu-CuS HSs hydrogel (equivalent to Au-CuS) without NIR laser irradiation.

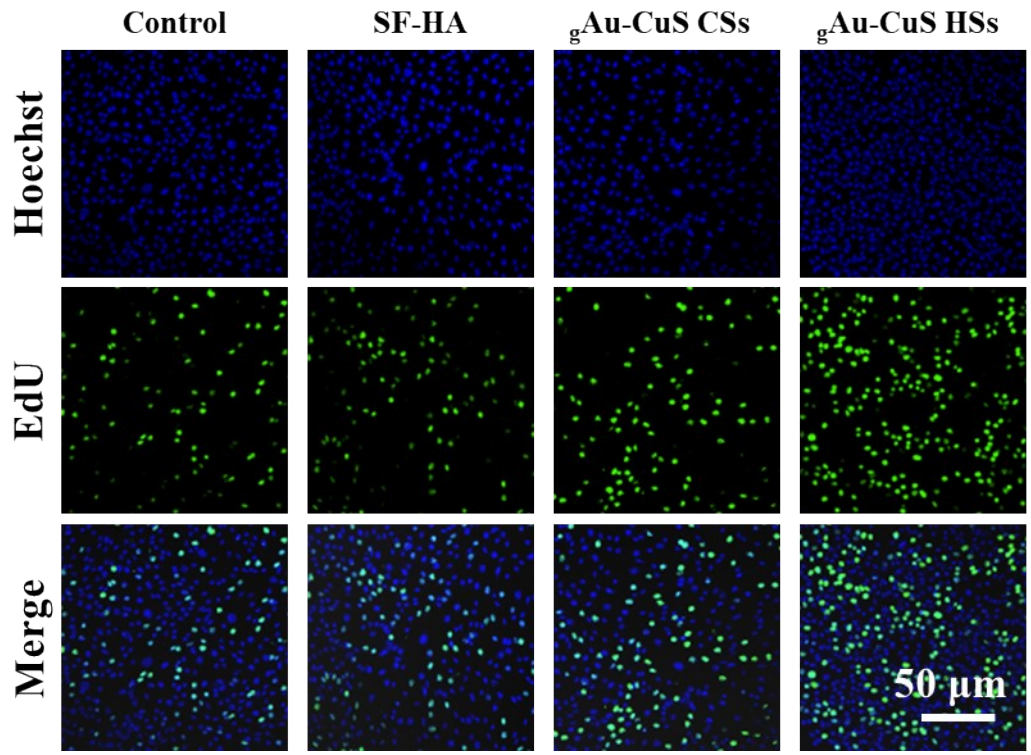

Figure S25. Cell proliferation after treatment with 100 μg mL^{-1} gAu-CuS CSs hydrogel and gAu-CuS HSs hydrogel (equivalent to Au-CuS) without NIR laser irradiation.

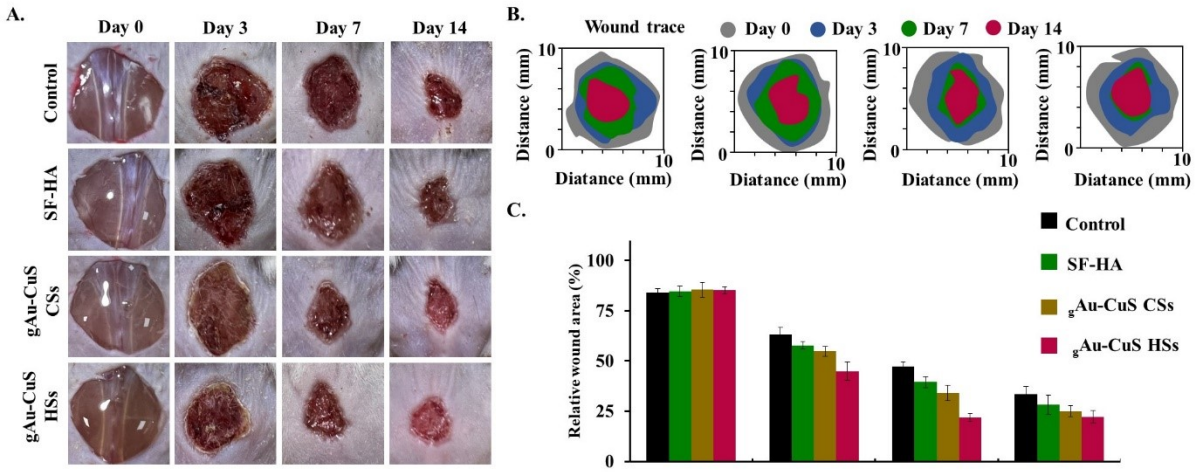

Figure S26. (A) Wound images of diabetic mice treated with 100 μg mL^{-1} gAu-CuS CSs hydrogel and gAu-CuS HSs hydrogel (equivalent to Au-CuS) without NIR laser irradiation. (B) Corresponding wound closure marks for 14 d of treatment. (C) *In vivo* wound closure rates at different time points in the four groups.

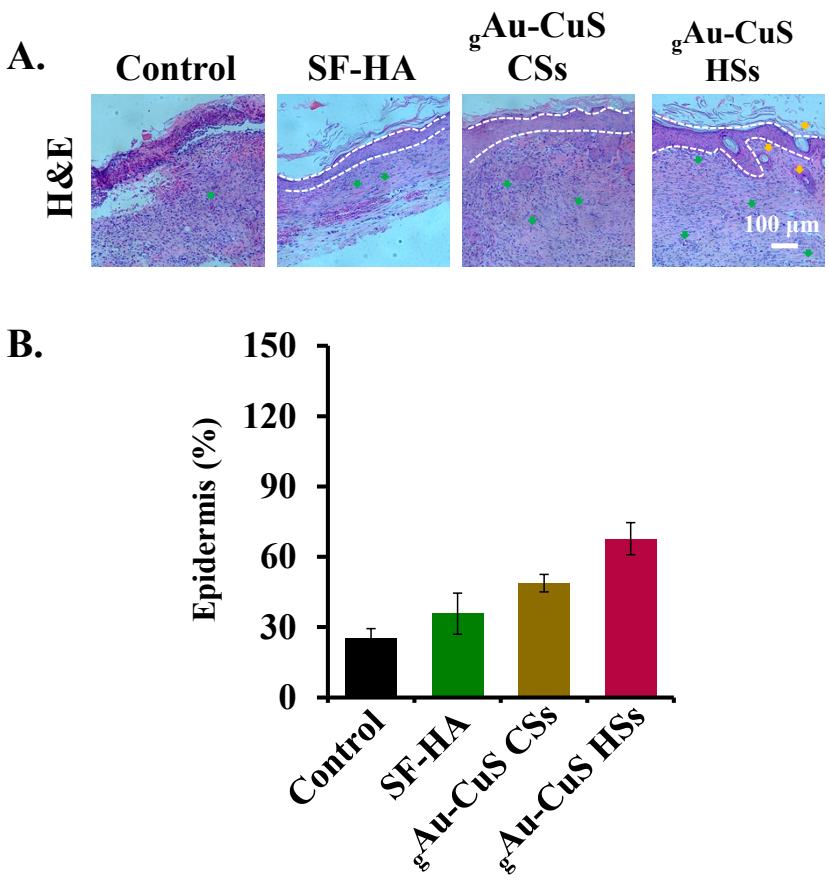

Figure S27. Without NIR illumination, H&E staining of wound tissue (A) and quantification of granulation tissue thickness (B) in in diabetic mice at day 14.

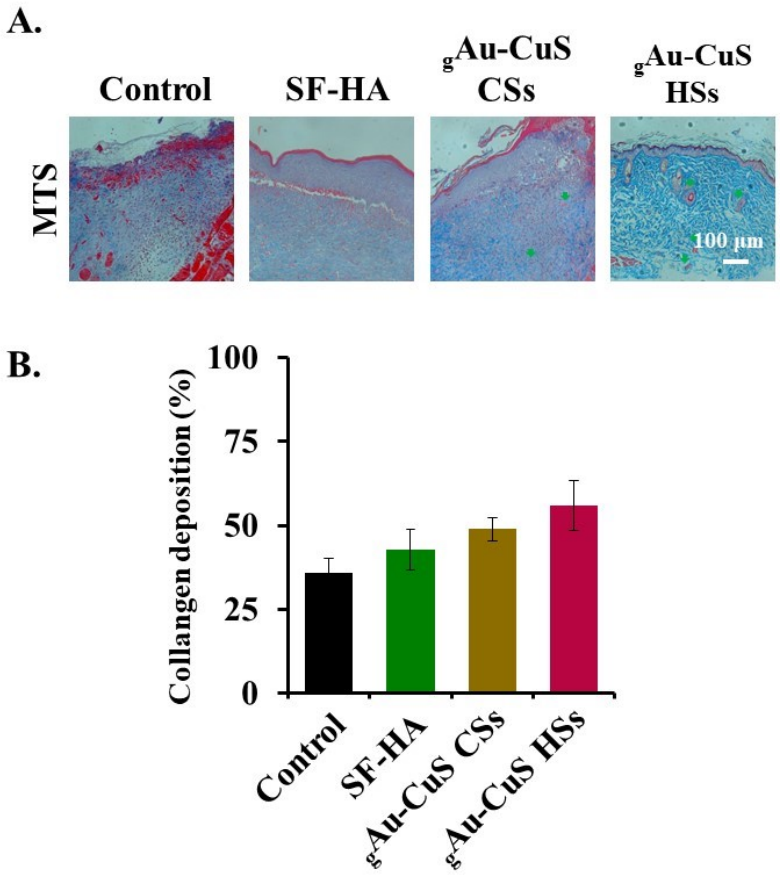

Figure S28. MTS staining without NIR illumination (A) and collagen quantification (B) of the wound tissue of diabetic mice at the 14 d.

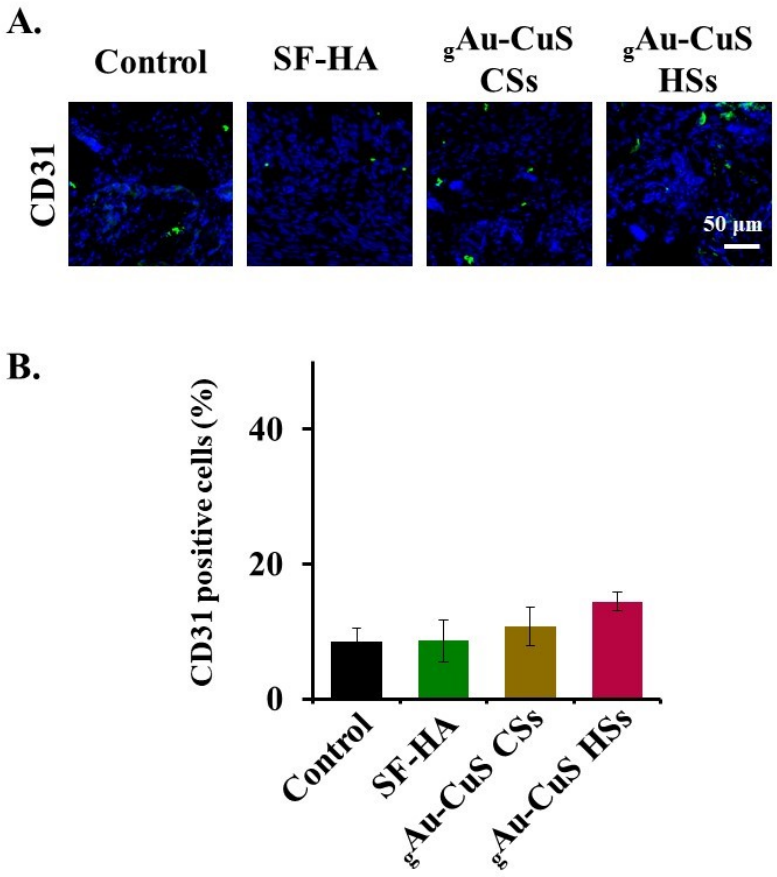

Figure S29. Without NIR illumination, (A) Immunofluorescence staining of CD31 (Green) and nuclei (blue) at day 14; (B) Quantitative analysis of the relative coverage area of CD31 for different groups.

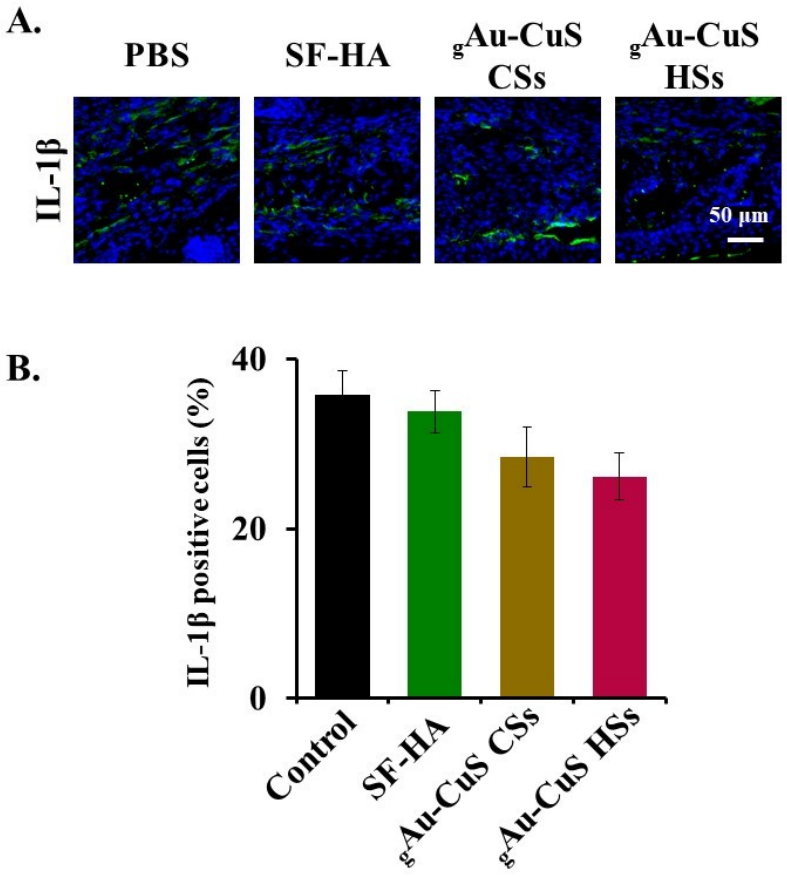

Figure S30. Without NIR illumination, (A) Immunofluorescence staining of IL-1β (Green) and nuclei (blue) at day 14; (B) Quantitative analysis of the relative coverage area of IL-1β for different groups.

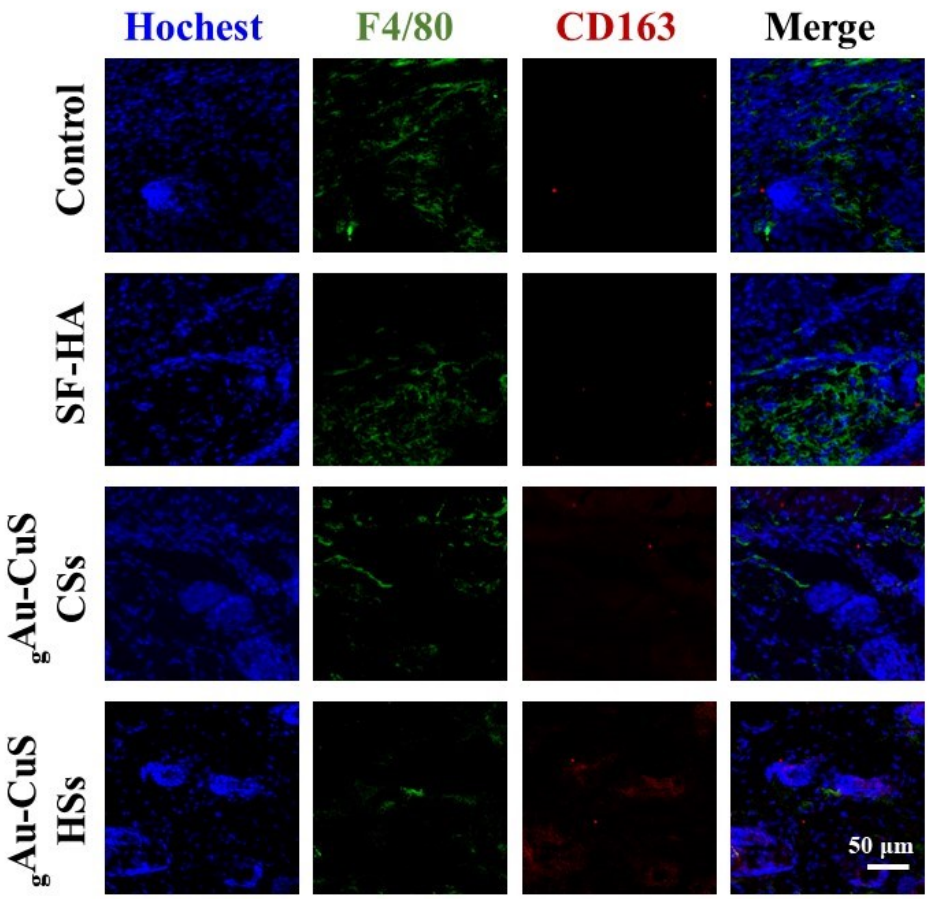

Figure S31. Without 808 nm laser irradiation (0.75 W cm^{-2}, 10 min), immunofluorescence images of macrophages in wound tissue after treatment, stained with F4/80 (green) and CD163 (red). Nuclei were stained with Hoechst (blue).

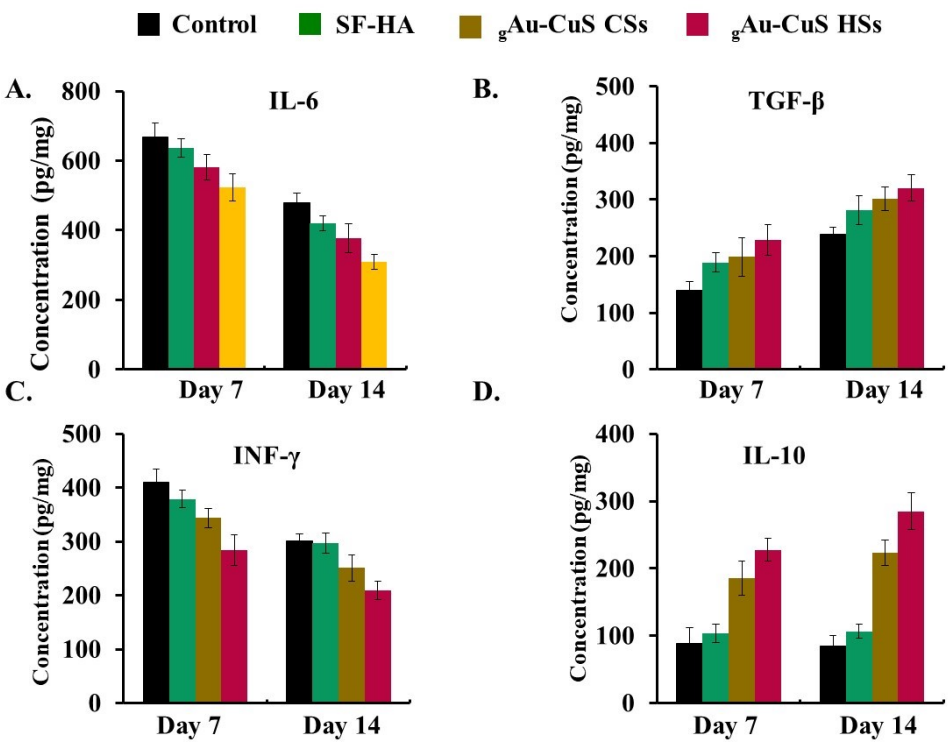

Figure S32. Without NIR illumination, analysis of IL-6 (A), TGF-β (B), IFN-γ (C) and IL-10 (D) levels in wounds of diabetic mice at 7 and 14 d.

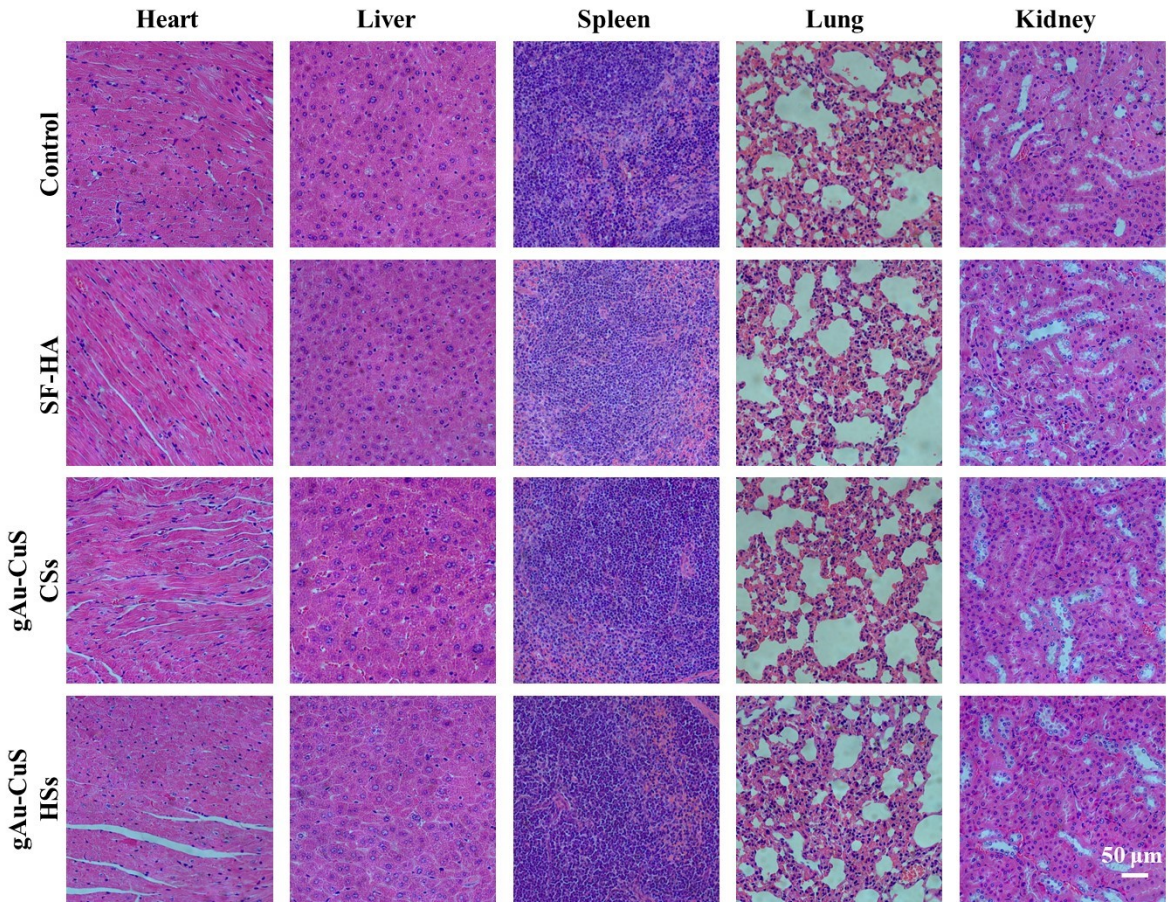

Figure S33. H&E-stained histological images of major organs collected at the end of treatment with 808 nm laser irradiation (0.75 W cm^{-2}, 10 min).

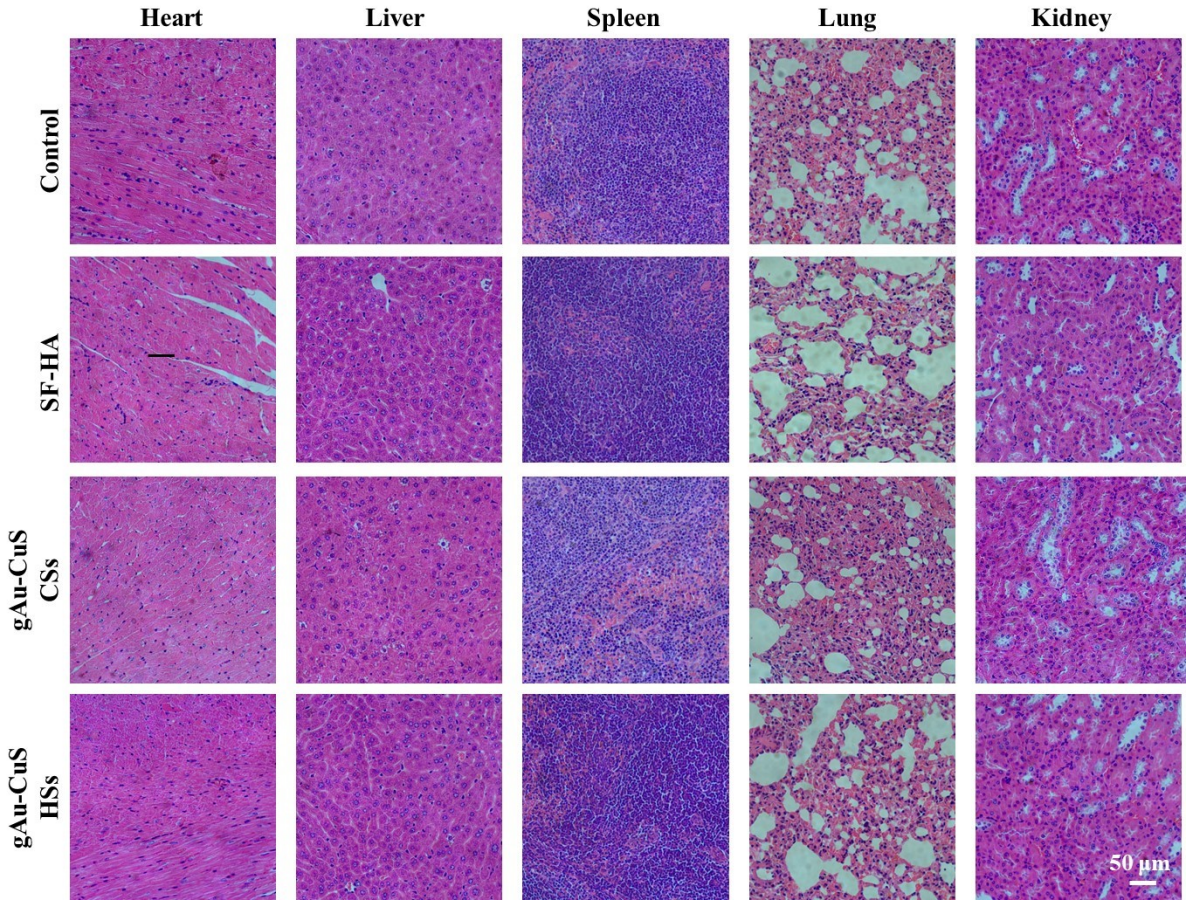

Figure S34. H&E-stained histological images of major organs were collected at the end of treatment without 808 nm laser irradiation.